Mineralogical and chemical characterization of an oolitic iron ore, and sustainable phosphorus removal

by W. Bendaikha[1], S. Larbi[2], and A. Ramdane[3]

Affiliation:
[1]Centre de développement des Energies Renouvelables, BP. 62 Route de l'Observatoire Bouzareah, 16340, Algiers, Algeria.
[2]LGMD- Department of Mechanical Engineering, Ecole Nationale Polytechnique 10, Avenue Hassen Badi, BP 182, El-Harrach, 16200, Algiers, Algeria.
[3]Scanning Electron Microscope Laboratory, Sonatrach laboratories division DLAB, Boumerdes, Algeria.

Correspondence to:
W. Bendaikha

Email:
w_bendaikha@yahoo.com
o.bendaikha@cder.dz

Dates:
Received: 17 Mar. 2022
Revised: 31 Oct. 2022
Accepted: 11 Dec. 2023
Published: February 2024

How to cite:
Bendaikha, W., Larbi, S., and Ramdane, A. 2024
Mineralogical and chemical characterization of an oolitic iron ore, and sustainable phosphorus removal.
Journal of the Southern African Institute of Mining and Metallurgy, vol. 124, no. 2. pp. 59–66

DOI ID:
http://dx.doi.org/10.17159/2411-9717/2051/2024

ORCID:
W. Bendaikha
http://orcid.org/0000-0001-5869-1404
S. Larbi
http://orcid.org/0000-0002-4382-4646
A. Ramdane
http://orcid.org/0009-0005-5509-3376

Synopsis

An oolitic iron ore from Gara Djebilet, Algeria was characterized by X-ray diffraction, scanning electron microscopy, and energy dispersive spectrosopy and the phosphorus distribution between various phases studied. Two ore types were identified – a haematite-dominated, oolitic type and a more massive, magnetite-dominated type. The haematite-dominated ore had a higher phosphorus content, up to 0.6% in the iron oxide minerals, than the magnetite-dominated type (0.3% P). Owing to the very fine-grained texture of the gangue minerals, reducing the phosphorus content to levels suitable for steelmaking (below 0.05% P) by conventiobal means would entail an energy-intensive process with a high carbon footprint. Preliminary leaching test work using a sulphurous geothermal water as lixiviant, assisted by solar thermal acceleration, gave very promising results, removing 0.13% of the residual P (or 21.7% removal of total P) from the high-phosphorus oolitic ore.

Keywords

Oolitic iron ore, phosphorus removal, renewable resources, sustainability, sulphurous thermal water, leaching, solar thermal.

Introduction

Algeria holds one of the richest oolitic ironstone deposits in North Africa (Diab *et al.*, 2020). Removal of phosphorus from these ores using conventional beneficiation methods is not possible (Tang *et al.*, 2017), owing to poor selectivity and recoveries, and low economic efficiency (Pownceby *et al.*, 2019). However, the increase in the international iron ore price in recent years has forced steel companies in many countries, such as FERAAL and MANAL in Algeria, to seek domestic sources of iron ore in order to reduce costs (Chen and He, 2014; Chen and Chu, 2014).

Many of the world's current iron ore resources contain over 0.08 wt% P, and are thus not suitable for iron- and steelmaking (Delvasto *et al.*, 2008; Cheng *et al.*,1999). Phosphorus increases the hardnessof iron and decreases the solubility of carbon in iron at high temperatures. This decreases its usefulness in making blister steel (cementation), where the speed and amount of carbon absorption is the overriding consideration affecting the economics of the ironmaking process and the quality of the produced steel (Song, 2013).

Previous workers have investigated the adsorption mechanisms of phosphorus and other impurities by goethite-rich iron ores in order to identify a possible removal method. Parfitt and Atkinson (1976) found that phosphate adsorption on synthetic goethite results in the formation of a binuclear complex. Omran *et al.* (2015) investigated phosphorus removal from three different iron ore samples with varying total iron and P_2O_5 contents and mineralogical textures, using combined microwave pretreatment and ultrasonic treatment. Their findings indicated that microwave pretreatment increases the efficiency of ultrasonic disintegration of gangue particles by about 20%. Depending on the sample texture and phosphorus distribution about 59% phosphorus removal could be obtained.

Liu *et al.* (2017) applied the slag ion theory to calculate the distribution ratio of phosphorus in the smelting reduction of high-phosphorus iron ores. They found that the main factors affecting the distribution ratio of phosphorus are ferrous oxide activity, phosphorus capacity of the slag, and the phosphorus activity coefficient in molten iron.

Quast (2018) reviewed the techniques that can be used for economically processing oolitic iron ores containing high levels of impurities, notably phosphorus.

Pownceby *et al.* (2019) investigated the distribution and association of phosphorus within goethite in a high-P Brockman-type iron ore from the Pilbara region of Western Australia. They concluded that

limited removal of phosphorus by physical separation techniques is possible, but will most likely result in a significant loss of iron units. Chemical leaching is also possible, but this approach is only successful after thermal pretreatment to recrystallizse the goethite as Fe_2O_3 and consequent concentration of impurities at grain boundaries.

Da Siva *et al.* (2020) used a kinetic model of heating using microwave energy in the acid baking/leaching process to reduce particulate phosphorus content in iron ores. Their results indicated that with microwave energy as a heating source, 600°C is the optimum temperature for promoting the diffusion of leaching agent within the iron ore particles.

Yehia (2021) investigated the use of a fungal cellulase enzyme to improve the selective separation of apatite from haematite during reverse anionic flotation of a high-phosphorus iron ore. The results showed that the enzyme was adsorbed on the surfaces of both minerals. However, the depressant effect was significant in the case of haematite, but not apatite.

The Gara Djebilet field (Figures 1 and 2) is an important deposit situated in the North African Palaeozoic ironstone belt in southwestern Algeria. It extendeds from Zemmour to Libya and includes ironstones of Ordovician, Silurian, and Devonian age (Guerrak,1988; Diab *et al.*, 2020).

In this investigation we studied the structural, microstructural, and chemical characteristics of this oolitic iron ore in detail in order to identify the nature of phosphorus inclusions in the ore, and carried out leaching tests with sulphurous geothermal water within a low-temperature solar greenhouse thermal acceleration system.

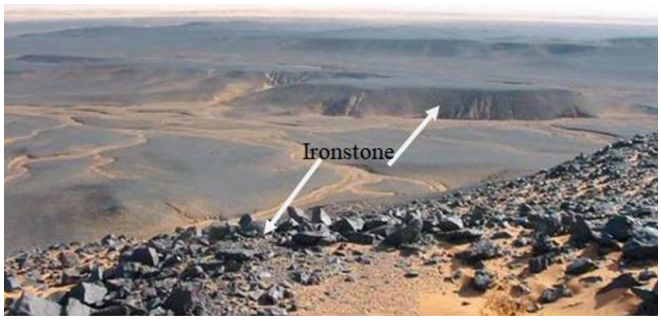

Figure1—North African Palaeozoic Ironstone belt, Gara Djebilet field

Materials and methods

Sample identification

Representative samples were selected, identified, and classified according to their morphology, weight, and colour. Two types of ore were identified, type A (haematite-dominated) and type B (magnetite-dominated).

The samples were crushed and pelletized in the following steps:

- Stagewise crushing in a series of jaw crushers with different slot openings:

Figure 2—Location of Gara Djebilet in the Tindouf Basin (SW Algeria)

- 50–20 mm
- 20–10 mm
- 5 mm.

➤ Roller crusher with an opening of 1 mm
➤ Drying at 105°C
➤ Quartering to obtain representative samples A and B.

After quartering, the representative samples were ground to a particle size of 90–70 µm using a disc mill.

Mineralogical and chemical analysis was carried out using X-ray diffraction (XRD), scanning electron microscopy (SEM), and energy dispersive spectroscopy (EDS) to investigate the structural complexity of each sample and to determine the phosphorus content.

Preliminary geothermal water leaching test

Sulphurous thermal water extracted from Hammam Righa, a geothermal spring located in northern Algeria, was used as a leaching solution in order to reduce the phosphorus content. The chemical composition of the water is given in Table I. A 'bottle drip leaching' set-up (Figure 3) was used tor the test, which requires 500 g of material.

Geothermal spring water from the Hammam Righa region is a sulphated-acid water with high concentrations of $(SO_4)^{2-}$ and Cl^- ions.

Figure 4 shows the greenhouse solar heating system used to treat sample A (phosphorus content 0.6%), for a period of 6 hours (from 9 a.m. to 3 p.m. the time of maximum solar insolation) in order to accelerate the geothermal water absorption process, and to dry the sample after soaking prior to grinding in a disc mill. The process was repeated six times.

Results and discussion

X-ray powder diffraction (XRD)

As shown in Figure 5, the minerals present in sample A are haematite (Fe_2O_3) in association with magnetite (Fe_3O_4), goethite (FeO(OH)), kaolinite ($Al_2Si_2O_5(OH)_4$), and montmorillonite ($(Na, Ca)_{0,3}$ $(Al, Mg)_2$ $Si_4O_{10}(OH)_2$ nH_2O).

Table I

Chemical composition (mg/l) of Hammam Righa geothermal water (Belhai *et al.*, 2016)

T (°C)	pH	Ca	Mg	Na	K	Cl	SO_4	HCO_3	SiO_2
68	6.5	470.4	47.7	220	9.4	370.6	1091.7	280	48.6

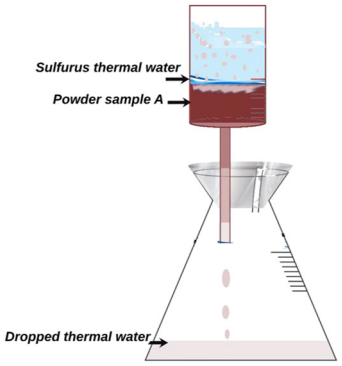

Figure 3—Set-up for bottle drip leaching

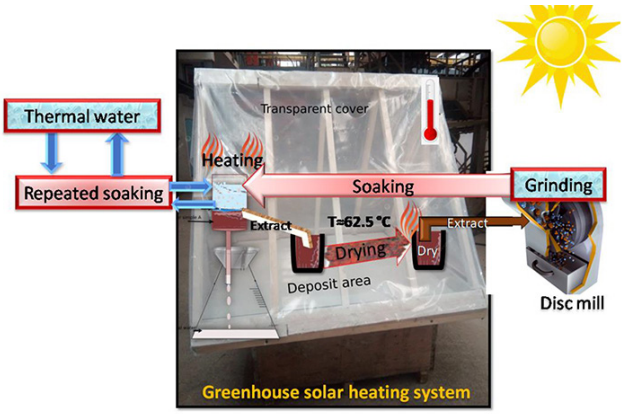

Figure 4—Greenhouse solar heating system

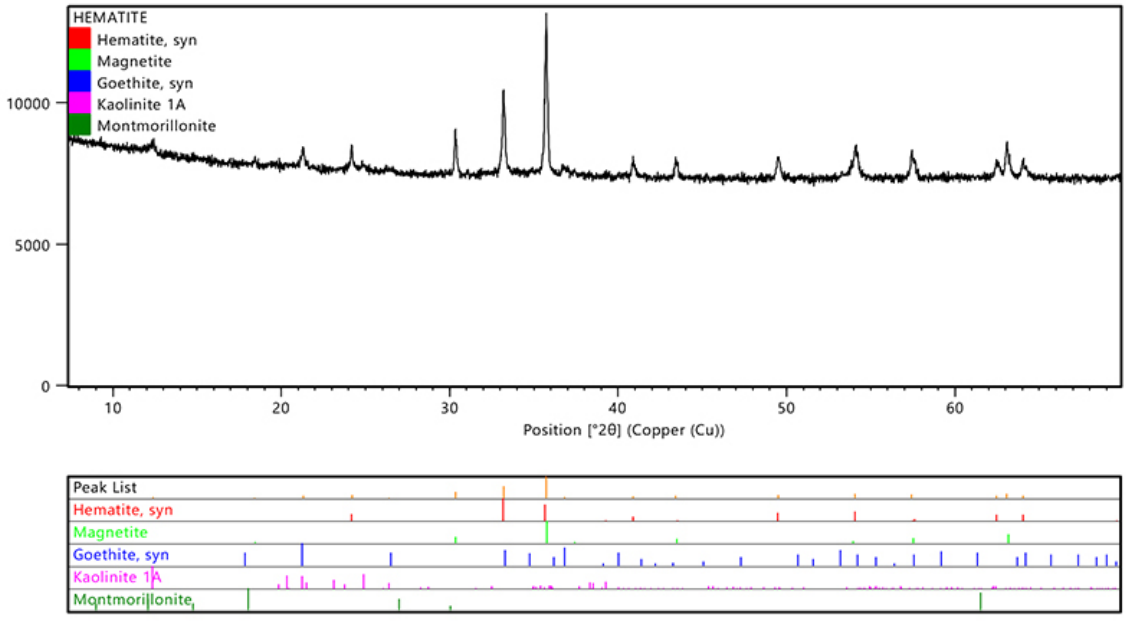

Figure 5—XRD spectrum of sample A

Sample B, as shown in Figure 6, is mainly composed of magnetite (Fe_3O_4) in combination with haematite (Fe_2O_3), chamosite, which is an iron-rich chlorite ($(Mg,Al,Fe)_{12}$ $[(Si,Al)_8O_{20}](OH)_{16}$), and clinochlore ($(Fe,Mg,Al)_6(Si,Al)_4O_{10}(OH)_8$).

Mineralological analysis

The mineralogical compositions of samples A and B are given in Tables II and III respectively. The polished section of sample A (Figure 7A) is characterized by a massive texture with a nodular or oolitic structure with 60% haematite content, 20% sub-automorphic magnetite, and 5% iron hydroxides in the form of a coating, giving the rock a reddish hue.

Sample B (Figure 7B) is characterized by a massive texture with a granular, nodular, and auto-morphic structure and major mineralogical components consisting of 60% massive automorphic magnetite, 25% oolitic haematite, and traces of xenomorphic pyrite.

Optical microscopy

Observation of the polished section of sample A showed haematite in association with magnetite and goethite. The haematite mineralization (Figure 7A) consists of oolites ranging in size from 0.05 to 10 mm. The oolite cores contain iron hydroxide (goethite) and gangue minerals.

Magnetite crystalline structure is automorphic (Figure 7B) with size ranging from 0.1 to 0.3 mm. Magnetite also occurs as irregularly nodules in the rock. The iron hydroxide is visible as a red coating.

The study of the polished section of sample B shows a rock rich in magnetite and haematite, which are associated with small amounts of pyrite. Figure 8A illustrates magnetite oolite and massive magnetite. Figure 8B shows the magnetite, which represents around 60% of the total volume of the rock. It clearly shows haematite with a goethite core and massive magnetite.

The results give us idea of the intermolecular phosphorus inclusions in haematite, magnetite, and possibly in goethite (Parfitt,1976), as well as in the gangue minerals. In order to determine the location and concentration of the phosphorus inclusions, further analysis using SEM and EDS spectra is required.

SEM analysis

The samples were dehydrated and processed to become electrically conductive. The pressure inside the instrument reaches a value of 2.99 10^{-3} Pa (2.99 10^{-8} bar). Energy-dispersive X-ray spectroscopy (EDS) analysis was used to determine the elements contained in the iron oxide ore.

Table II

Mineralogical composition of sample A

Mineralogical composition	Content (%)	Grain form	Grain size (mm)
Haematite	60	Oolitic	0.05–10
Magnetite	20	Subautomorphic	0.05–0.5
Iron hydroxide (goethite)	05	Coating	–

Table III

Mineralogical composition of sample B

Mineralogical composition	Content (%)	Grain form	Grain size (mm)
Magnetite	60	Massive-automorphic	0.05-10
Haematite	25	Oolitic	0.05-03
Pyrite	01	Xenomorph	0.02-0.1

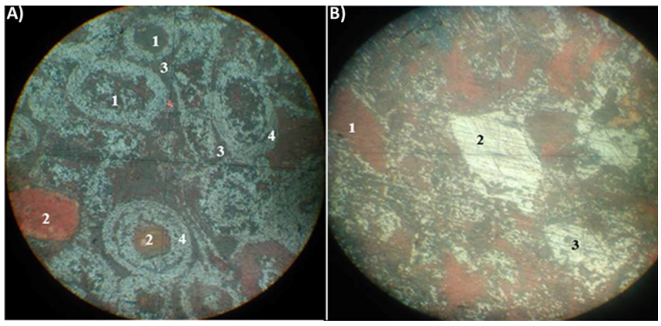

Figure 7— (A) Oolitic haematite showing (1) core gangue, (2) goethite, (3) inter-oolitic space composed of gangue minerals, (4) oolitic haematite. Polarized light, 20× magnification. (B) Magnetite automorphic, showing (1) goethite, (2) automorphic magnetite, (3) subautomorphous magnetite. 20× magnification

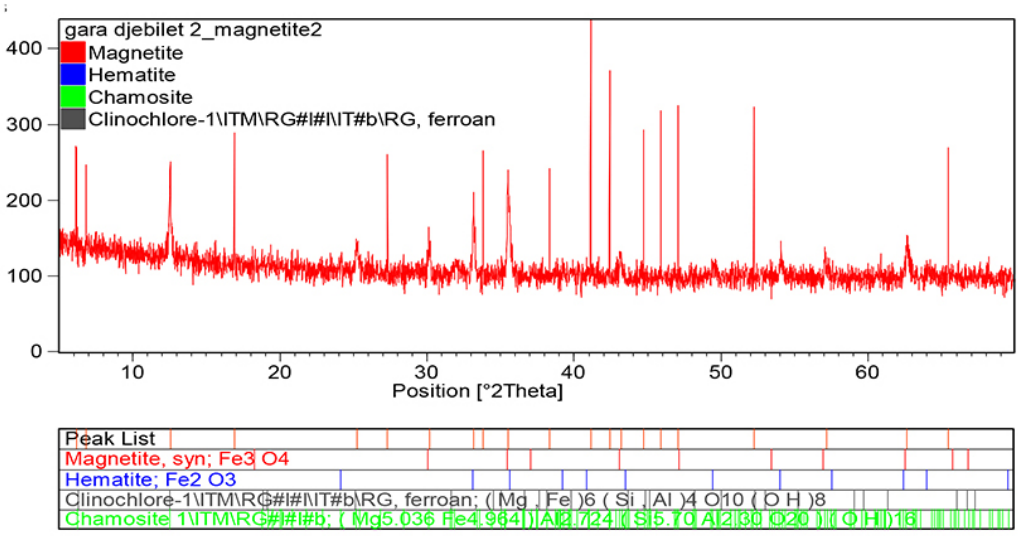

Figure 6—XRD spectrum of sample B

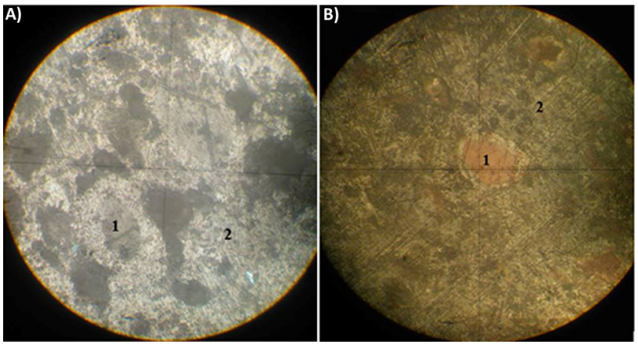

Figure 8—(A) Microstructure of a magnetite-containing oolitic haematite, showing (1) magnetite oolite and (2) massive magnetite. 20× magnification. (B) Massive magnetite containing (1) hsematite with a goethite core and (2) massive magnetite. 20× magnification

Results of sample A

Sample A was examined at magnifications from 500 µm to 10 µm. The thin section of haematite shown in Figure 9A depicts a regular spherical oolitic form consisting of a core around which concentric shells have developed by chemical (or biochemical) precipitation. The same grain at higher magnification is shown in Figure 9B. Three typical zones were selected: marked as 1 (haematite), 2 (core), and 3 (gangue minerals).

Figure 9C is a view of of zone 2 (Figure 9B), showing (1) haematite, (2) magnetite microinclusions occuring as octahedral crystals bounded by planes and rhombic dodecahedra, and (3) phyllosilicates flakes. Figure 9D shows the core at 10 µm scale; the phyllosilicates flakes are clearly observed.

The EDS analysis of the oolite grain in Figure 9B is shown in Tables IV, V, and VI. It can be seen that the haematite in zone 1

Table IV

EDS results for zone 1

Element	%mass	%atomic	Total intensity	Error%	K-ratio
C K	2.31	5.80	58.69	10.75	0.0077
O K	29.78	56.06	2419.79	5.46	0.2097
Al K	1.52	1.7	100.75	7.85	0.0084
Si K	0.71	0.76	57.06	7.94	0.0049
P K	0.60	0.58	41.75	7.58	0.0046
Fe K	65.07	35.09	1244.45	2.59	0.5867

(Table IV) has a composition of about 65.07% iron and 29.78% oxygen by weight. The main impurities are a mixture of 2.31% C, 1.52% Al, 0.7% Si, and 0.6% P.

The results for zone 2, the core (Table V), show that the iron content is lower than in zone 1, with 14.13% Fe and a very high oxygen content (46.71%), which indicates the presence of goethite (FeO(OH)); This zone also contains 0.5% P, 6.84% Si, 12.03% Al, 18.21% C, and 1.13% Mg.

However, in the gangue minerals, zone 3 (Table VI), the phosphorus content is lower than in zones 1 and 2, at only 0.19 %, the iron is 29.23%, and the carbon, calcium, (from hydroxyapatite $Ca_{10}(PO_4)_6(OH)_2$) and oxygen contents are 42.38%, 0.22%, and 24.32%, respectively.

Results of sample B

SEM observations of sample B reveal a completely different microstructure to sample A, with recrystallization of haematite and apatite within the core. The iron-rich radiating lamellae can be seen in Figure 10A. The three-dimensional microstructure of sample B is illustrated in the SEM image in Figure 10B.

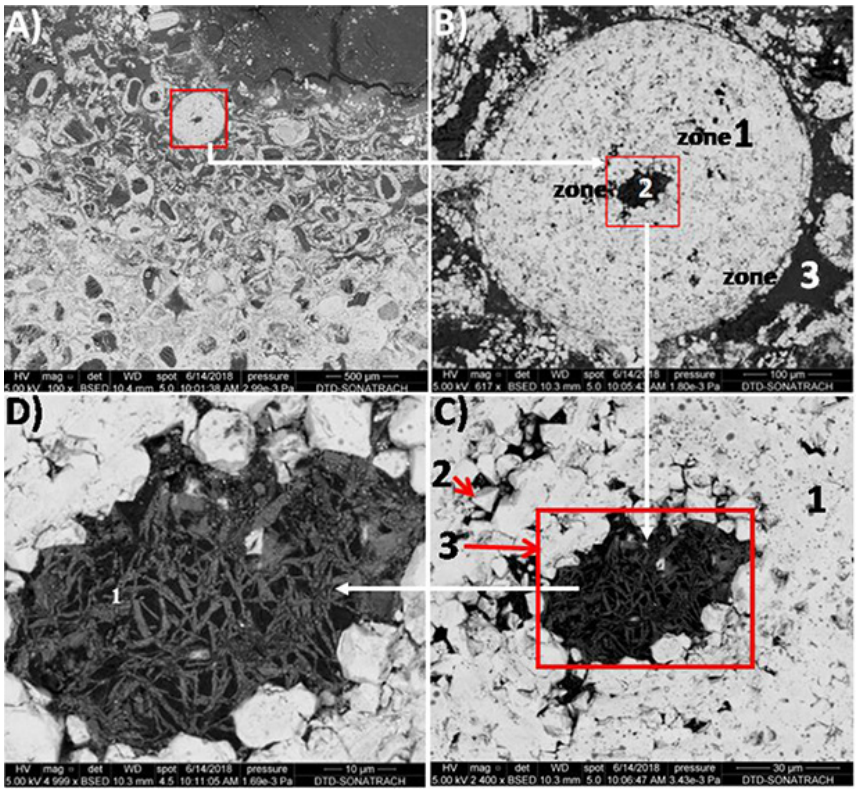

Figure 9—SEM micrographs of haematite. (A and B) oolitic haematite, (C) oolite core with magnetite inclusions, (D) lamellar structure of core

Table V

EDS results for zone 2

Element	%mass	%atomic	Total intensity	Error%	K-ratio
C K	18.21	27.80	249.52	9.28	0.0483
O K	46.71	53.53	1623.54	7.17	0.2064
Fe K	14.13	4.64	114.58	8.33	0.0473
Mg K	1.13	0.85	54.33	7.33	0.0065
Al K	12.03	8.17	654.75	4.45	0.0802
Si k	6.84	4.47	383.72	4.55	0.0482
P K	0.50	0.29	22.18	14.86	0.0036
S K	0.16	0.09	7.47	26.19	0.0013
Cl K	0.28	0.15	11.75	18.29	0.0023

Table VI

EDS results for zone 3

Element	%mass	%atomic	Total intensity	Error%	K-ratio
C K	42.38	61.78	764.80	7.64	0.1786
O K	24.32	26.61	481.59	8.73	0.0738
Na K	0.22	0.17	4.76	25.49	0.0008
Mg K	0.42	0.31	15.29	10.11	0.0022
Al K	1.04	0.68	44.05	6.8	0.0065
Si K	0.79	0.49	38.58	6.19	0.0058
P K	0.19	0.11	7.57	21.79	0.0015
S K	0.23	0.12	9.28	18.26	0.0019
Cl K	0.96	0.47	34.79	6.60	0.0081
Ca K	0.22	0.10	5.55	23.62	0.0021
Fe K	29.23	9.16	283.23	2.95	0.2351

The EDS spectra show that sample B is mainly composed of iron (62.08%) and oxygen (26.78%), with 7.21% C, 1.04% Al, 0.93% Si, and less phosphorus (0.3%) than in sample A. There are also fewer inclusions of Na (0.39%), Mg (0.39%), S (0.16%), Cl (0.16%), K (0.1%), Ca (0.23%), and Ti (0.22%). It has been observed that when the oxygen content is lower, the phosphorus content is also lower.

Preliminary results of experimental geothermal water leaching

The geothermal springs host several habitats, including thermal water, biofilms, and sediment (Chen *et al.*, 2023). The sulphurous thermal water used In this investigation contains a variety of

Table VII

EDS results for sample B

Element	%mass	%atomic	Total intensity	Error%	K-ratio
C K	7.21	17.04	128.97	9.3	0.0207
O K	26.78	47.52	1509.40	6.89	0.1303
Na K	0.39	0.49	8.88	20.11	0.0007
Mg K	0.39	0.46	17.47	13.73	0.0012
Al K	1.04	1.09	65.02	8.67	0.0043
Si K	0.93	0.94	78.78	7.49	0.0052
P K	0.30	0.27	23.84	8.53	0.0019
S K	0.16	0.14	14.25	15.60	0.0012
Cl K	0.16	0.13	14.53	13.22	0.0013
K K	0.10	0.07	7.91	26.54	0.0009
Ca K	0.23	0.17	17.12	11.29	0.0023
Ti K	0.22	0.13	14.95	10.56	0.0021
Fe K	62.08	31.56	2411.59	1.60	0.5623

dissolved minerals, as shown in Table I, and according to previous studies, it contains elementary sulphur-oxidizing bacteria (Culivicchi., 2005) which facilitate two simultaneous processes:

$$2H_2S + O_2 \rightarrow 2S + 2H_2O \quad [1]$$

$$2S + 3O_2 = 2H_2O \rightarrow 2SO_4^{2-} + 4H^+ \quad [2]$$

These bacteria proliferate at temperatures between 55°C and 85°C (Culivicchi-, 2005), and metabolize oxygen and inorganic phosphorus. Therefore, these essential elements (oxygen and phosphorus) available in this iron ore can be dissolved and eliminated at the same time.

A low-temperature leaching process using water from Hammam Righa was investigated with the aim of reducing the level of harmful phosphorus in oolitic iron ore in an eco-friendly manner.

A 500 g portion of sample A, with a particle size varying between 70 and 90 µm, and an initial phosphorus content of 0.6% (by weight) was used in the test. The sample was contacted with the thermal water for six consecutive days. On each day, the sample was well mixed and placed in the solar thermal heating system for 6 hours, from 9 am to 3 pm (maximum solar insolation). At the end of the experiment, the sample was dry and the temperature inside the solar heating system was approximately 62.5°C. The sample was then finely ground in a disc mill, and contacted again with the thermal water. This process was repeated six times.

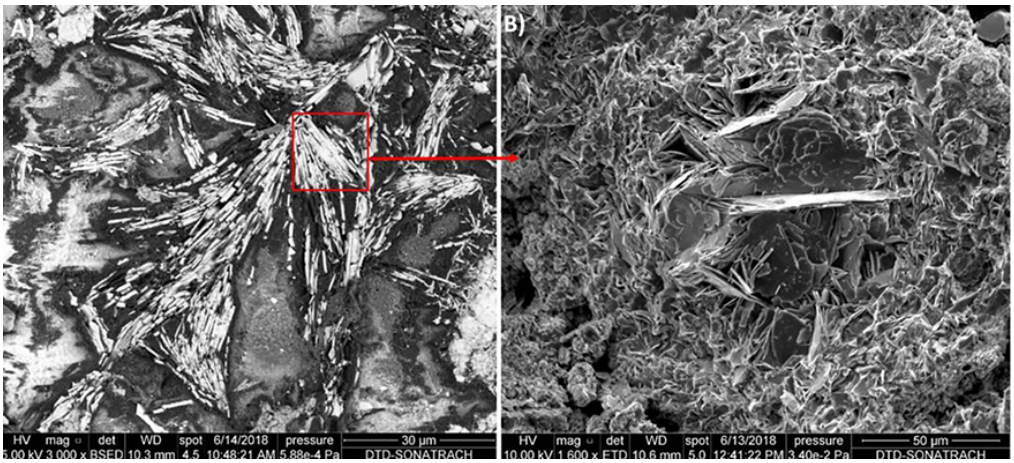

Figure 10—(A) Radiating iron-rich lamellae, (B) textural organization of magnetite

Sulphuric acid dissolves phosphorus in the iron-rich minerals and gangue minerals as follows:

$$Ca_3(PO_4)_2 + 3H_2SO_4 + 3nH_2O \rightarrow 2H_3PO_4 + 3CaSO_4 \cdot nH_2O \downarrow \quad [3]$$

$$Ca_3(PO_4)_2 + 2H_2SO_4 + 2nH_2O \rightarrow Ca^{2+} + 2H_2PO_4^- + 2CaSO_4 \cdot nH_2O \quad [4]$$

The Fe in solution is reduced from Fe^{3+} to Fe^{2+} (Dong *et al.*, 2019):

$$H_2S + Fe_2(SO_4)_3 \rightarrow H_2SO_4 + 2FeSO_4 + S \quad [5]$$

$$2H_2SO_4 + 4Fe(SO_4) + O_2 \rightarrow 2Fe_2(SO_4)_3 + 2H_2O \quad [6]$$

$$FeS_2 + 14Fe^{3+} + 8H_2O \rightarrow 15Fe_2^+ + 2H_2SO_4 + 12H^+ \quad [7]$$

The thermal solution contain iron ions, sulphate ions SO_4^{2-} and dissolved phosphorus as PO_4^{2-}.

$$2(3H^+(PO_4^-)) + Fe^{3+} + PO_4^{3-} \rightarrow Fe^{3+} + 6H^+ + 3PO_4^{2-} \quad [8]$$

The results are summarized in Table VIII. This experiment was repeated three times, and the same results were obtained with a small margin of error.

These preliminary results are encouraging, with 0.13% P removal, representing a removal ratio of 21.7%.

Conclusion and recommendations

The mineralogy, microstructure, and chemical composition of a high-phosphorus oolitic iron ore from Gara Djebilet in Algeria were investigated. Two types of ore were identified, A (haematite-dominated) and B (magnetite-dominated), with distinctly different microstructures. Type A ore had the higher phosphorus content, 0.6% compared with 0.3% for type B. The phosphorus content is proportional to the Fe and O contents, indicating that P is largely substituted in goethite.

Preliminary test work to reduce the phosphorus content of the haematite-dominated ore by solar-assisted leaching in sulphurous geothermal water yielded promising results, wirh 21.7% phosphorus removal. The sulphur in the geothermal water is produced by sulphur-oxidizing bacteria at temperatures of 55–85°C. The use of a bioleaching process to improve the P removal ratio is a possible topic for future investigations.

Acknowledgements

The authors would like to thank Mr Yahia Azeri, President General Manager of the National Office of Geological and Mining Research (ORGM, Boumerdès, Algeria) for his interest and his help in carrying out this study. Special thanks are extended to Mr Hassini, Mrs Karima Almouboudi, Mr N. Mendiliand, Mr O. Belgaid, and K. Snoussi, the staff of the National Office of Geological and Mining Research (ORGM, Boumerdès, Algeria) for their assistance with the experimental work.

Table VIII

Results of leaching tests using geothermal water

Fe total (%)	Solid (g)	Initial P (mass %)	P removal (%)	Error (three replications)
65.07	500	0.6	0.13	±0.15

References

Belhai, M., Fujimitsu, Y., Bouchareb-Haouchine, F.Z., Haouchine, A., and Nishijima, J. 2016. A hydrochemical study of the Hammam Righa geothermal waters in north-central Algeria. *Acta Geochimica*, vol. 35. pp. 271–287. https://doi.org/10.1007/s11631-016-0092-8

Champetier, Y., Hamdadou, E., and Hamdadou, M. 1987. Examples of biogenic support of mineralization in two oolitic iron ores - lorraine (France) and gara djebilet (Algeria). *Sedimentary Geology*, vol. 51. pp. 249–255. https://doi.org/10.1016/0037-0738(87)90050-9

Cheng, C.Y., Misra, V.N., Clough, J., and Mun, R. 1999. Dephosphorization of Western Australianiron ore by hydrometallurgical process. *Minerals Engineering*, vol. 9. pp. 1083–1092. https://doi.org/10.1016/S0892-6875(99)00093-X

Chen, G. and He, S. 2014. Thermodynamic analysis and experimental study of manganese ore alloy and dephosphorization in converter steelmaking. *Journal of the Southern African Institute of Mining and Metallurgy*, vol.114. pp. 391–399.

Chen, J-S., Hussain, B., Tsai, H-C., Nagarajan,V., Koner, S., and Hsu, B-M. 2023. Analysis and interpretation of hot springs water, biofilms, and sediment bacterial community profiling and their metabolic potential in the area of Taiwan geothermal ecosystem. *Science of the Total Environment*, vol. 856. pp. 159115. https://doi.org/10.1016/j.scitotenv.2022.159115

Chen, S.Y. and Chu, M.S. 2014. A new process for the recovery of iron, vanadium, and titanium from vanadium titanomagnetite. *Journal of the Southern African Institute of Mining and Metallurgy*, vol. 114. pp. 481–488.

Culivicchi, G., Lenzi,A., Tarquini,B., and Mariani, S. 2005. Sulfobacteria in geothermal fluids: a preliminary study in the Larderello geothermal area. *Proceedings of the World Geothermal Congress,* Antalya, Turkey, 24-29 April 2005. International Geothermal Association, Auckland, N.Z. https://www.geothermal-energy.org/pdf/IGAstandard/WGC/2005/0247.pdf

Da Siva, L.M., Nascimento, M., de Oliveira, E.M., de Queiroz, A.V., Fernandes, M.T., and de Castro, J.A. 2020. Evaluation of the diffusional coefficient in the acid baking process using microwave energy to reduce phosphorus content in iron ore particles. *Minerals Engineering*, vol. 157. pp. 106541. https://doi.org/10.1016/j.mineng.2020.106541

Delvasto, P., Valverde, A., Ballester, A., Muno, J.A., Gonzalez, F., Blazquez, M.L., Igual, J.M., and Garcia-Balboa, C. 2008. Diversity and activity of phosphate bioleaching bacteria from a high-phosphorus iron ore. *Hydrometallurgy,* vol. 92. pp. 124–129. https://doi.org/10.1016/j.hydromet.2008.02.007

Diab, H., Chouabbi, A., Chi Fru, E., Nacer D., and Krekeler, M. 2020. Mechanism of formation, mineralogy and geochemistry of the ooidal ironstone of Djebel Had, northeast Algeria. *Journal of African Earth Sciences*, vol. 162. pp. 103736. https://doi.org/10.1016/j.jafrearsci.2019.103736

Dong, Z., Zhu,Y., Han, Y., Gu,X., and Jiang, K. 2019. Study of pyrite oxidation with chlorine dioxide under mild conditions. *Minerals Engineering*, vol 133. pp. 106–114. https://doi.org/10.1016/j.mineng.2019.01.018

Elzinga, E.J. and Sparks, D.L. 2007. Phosphate adsorption onto hematite: An in situ ATR-FTIR investigation of the effects of pH and loading level on the mode of phosphate surface complexation. *Journal of Colloid and Interface Science*, vol. 308. pp. 53–70. https://doi.org/10.1016/j.jcis.2006.12.061

Guerrak, S. 1988. Geology of the Early Devonian oolitic iron ore of the Gara Djebilet field, Saharan Platform, Algeria. *Ore Geology Reviews*, vol. 3. pp. 333–358. https://doi.org/10.1016/0169-1368(88)90026-1

Liu, Y., Zhang, H., Li, Z., Zhang, A., Zhang, X., and Qing, S. 2017. Impact of slag composition activity on the behavior of phosphorus in the smelting reduction process of high-phosphorus iron ores. *International Journal of Hydrogen Energy*, vol. 42. pp. 24487–24494. https://doi.org/10.1016/j.ijhydene.2017.06.119

Omran, M., Fabritius, T., Elmahdy, A.M., Abdel-Khalek, N.A., and Gornostayev, S. 2015. Improvement of phosphorus removal from iron ore using combined microwave pretreatment and ultrasonic treatment. *Separation and Purification Technology*, vol.156. pp. 724–737. https://doi.org/10.1016/j.seppur.2015.10.071

Parfitt, R.L. and Atkinson R.J. 1976. Phosphate adsorption on goethite (α-FeOOOH). *Nature*, vol. 264. pp. 740–742. https://doi.org/10.1038/264740a0

Powneby, M.I., Hapugoda, S., Manuel, J., Webster, N.A.S., and MacRae, C.M. 2019. Characterisation of phosphorus and other impurities in goethite-rich iron ores – Possible P incorporation mechanisms. *Minerals Engineering*, vol. 143. pp. 106022. https://doi.org/10.1016/j.mineng.2019.106022

Quast, K. 2018. A review on the characterisation and processing of oolitic iron ores. *Minerals Engineering*, vol. 126. pp. 89–100. https://doi.org/10.1016/j.mineng.2018.06.018

Song, S., Campos-Toro, E.F., and Valdivieso, A.L. 2013. Formation of micro-fractures on an oolitic iron ore under microwave treatment and its effect on selective fragmentation. *Powder Technology*, vol. 243. pp. 155–160. https://doi.org/10.1016/j.powtec.2013.03.049

Tang, H., Fu, X., Qin, Y., and Qi, T. 2017. Iron recovery and phosphorus removal from oolitic high-phosphorus haematite. *Journal of the Southern African Institute of Mining Metallurgy*, vol. 117, no. 4. pp. 387–395. http://dx.doi.org/10.17159/2411-9717/2017/v117n4a11

Torres-Ceron, D.A., Acosta-Medina, C.D., and Restrepo-Parra, E. 2019. Geothermal and mineralogic analysis of hot springs in the Puracé-La Mina Sector in Cauca, Colombia. *Geofluids*, vol. 2019. pp. 1–4. https://doi.org/10.1155/2019/3191454

Yehia, A., Abd El-Halim, S., Sharada, H., Fadel, M., and Ammar, M. 2021. Application of a fungal cellulase as a green depressant of hematite in the reverse anionic flotation of a high-phosphorus iron ore. *Minerals Engineering*, vol. 167. pp. 106903. https://doi.org/10.1016/j.mineng.2021.106903 ◆